doi：10.3969/j.issn.2095-0411.2022.06.009

A System-Level Model of the Packaged Wind Sensor System

CHEN Bei

(School of Microelectronics and Control Engineering, Changzhou University, Changzhou 213164, China)

Abstract: A system-level model of the wind sensor system including the sensor chip and the conditioning circuit was proposed in this paper. The wind sensor was composed of a center temperature sensor, four heaters and four temperature sensors. The presented model was based on the theory of lumped parameters. An analogy was drawn between the heat flow and the electric current. Herein, the voltage is an analogy for the temperature, and the thermal resistance is the resistance in the thermal transfer like the resistance in the circuit. Further, the thermal analysis of the sensor chip and the electrical analysis of the conditioning circuit were developed in one system-level circuit by using the model. The test was performed in the wind tunnel. Experiment results presented here showed an agreement with the system-level model. The results presented here provided a valuable reference for the practical application of the wind sensor.

Key words: system-level model; thermal-electrical model; thermal wind sensor

已封装风速计系统的系统级模型研究

陈 蓓

（常州大学 微电子与控制工程学院，江苏 常州 213164）

摘要：设计了一个风速计系统的系统级模型，该风速计系统由传感器芯片和控制电路构成。风速传感器包括 1 个中心温度传感器、4 个加热条和 4 个测温传感器。文章提出的模型基于集总参数理论，将热流比拟为电流，电压比拟为温度，热传导过程中的热阻比拟为电路的电阻。利用这一系统级模型构建的系统级电路，可以同时进行传感器芯片的热学分析与控制电路的电学分析。测试在风洞中进行，实验结果与系统级模型具有良好的一致性，这一研究成果为风速计的实际应用提供了有价值的参考。

关键词：系统级模型；热电模型；热风速传感器

中图分类号：TN 4 **文献标志码**：A **文章编号**：2095-0411(2022)06-0075-09

收稿日期：2022-05-26。

作者简介：陈蓓(1988—)，女，江苏徐州人，博士，讲师。E-mail：chenbei@cczu.edu.cn

引用本文：CHEN Bei. A system-level model of the packaged wind sensor system[J]. 常州大学学报(自然科学版)，2022，34(6)：75-83.

The thermal wind sensor has been considered a promising technology due to its low cost, low power, small size, and no movability parts. For decades, it has been widely researched in different groups[1]. In the aspect of improving sensitivity, some pendent structures[2], membrane structures[3] and insulation trenches[4-5] were developed. In the aspect of reducing power consumption, not only these pendent structures but also some substrates with small thermal conductivity[6], such as glass[7] or porous silicon[8], were utilized. Besides, some circuit designs[9] were applied. In enlarging the measurement range, more sets of thermometers were manufactured on the chip[10-11]. Moreover, hybrid measurement modes, such as thermal anemometer and calorimetric[12], or calorimetric and time-of-flight[13], collectively control the sensor system. In reducing temperature drift, some compensation circuits and compensation models were developed[14-17]. In the process of researching the thermal wind sensor, the thermal analysis of the sensor chip usually were finished in FEM (Finite Element Method) simulation tools[18-20]. Whereas, the electrical analysis of the control circuit were independently finished in electrical EDA (Electronic Design Automation) tools[21]. However, the sensor chip and the conditioning circuit have interactions with each other. The conditioning circuit controls the heating power, that is to say, the temperature of the chip. Similarly, the chip temperature affect the electrical parameters of the thermometers resulting in the change of the state of the circuit. Unfortunately, wind-thermal-electric model of the thermal wind sensor system has not been explored. To our knowledge, SHEN et al. [22] developed a macro model of the sensor chip, unfortunately the encapsulation of the wind sensor was not considered in this model, which induced that the presented macro model did not conform to practical applications. In this paper, a new system-level model which contains the sensor chip and the encapsulation was presented. The new system-level is more convenient for practical analysis and applications.

In this paper, a system-level model of the thermal wind sensor system has been developed. By the theory of heat conduction and forced convection, the thermal resistances of the chip are examined. Based on the theory of the lumped parameters, the thermal circuit of the chip is developed. By combining the thermal circuit and the conditioning circuit, the system-level model has been established. This model can easily be analyzed in Cadence, and help researchers understand the work process of the sensor system and improve the conditioning circuit.

1 Description of the sensor system

Fig.1 shows the schematic diagram of the thermal wind sensor. The chip consists of a central thermistor, four central heaters and four outlying thermistors in four directions. The chip is adhered to the ceramic substrate to avoid the environmental contaminants. The backside of the chip is protected by thermal insulation glue. The ceramic substrate is pasted in the center of the black aluminum ring. Because of the high thermal conductivity, the aluminum ringtakes on the role of a thermal sink to keep the temperature of the ceramic edge at the ambient temperature. When the sensor chip is heated, the resulting heat transfers through two routes, i. e. thermal convection and thermal conduction as shown in Fig.1.

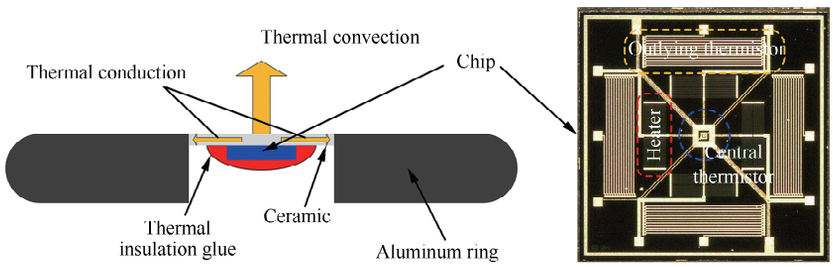

图 1　热风速传感器结构示意图

Fig.1　Schematic diagram of the structure of the thermal wind sensor

To control the heating and temperature measurement of the wind sensor, the conditioning control circuit of the sensor system is designed in Fig.2. The chip diode and the environment diode are placed in two branches of Wheatstone bridge respectively. The heating power of the heaters is controlled by R_5. In the initial condition, the sensor has the stable temperature. When wind speed increases, the temperature of the chip decreases due to the increasing thermal convection. As the diode has a negative temperature coefficient, the voltage of the chip diode will increase. Then the voltage of the negative input of the amplifier will increase. It will induce the decrease of the output voltage of the amplifier. Due to the action of the voltage regulator V_z, the current through R_6 will increase. The base current of the transistor will increase. As the transistor works in the amplification zone, the collector current will also increase. The increased heat power will make the chip temperature rise. This process becomes a negative feedback loop, and vice versa.

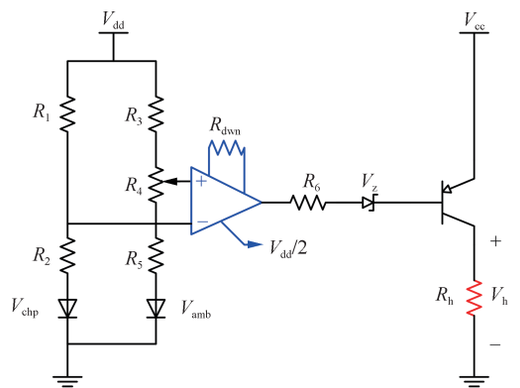

V_{chp}—the temperature sensor on the chip; V_{amb}—the outside temperature sensor; R_h—the heaters in parallel on the chip.

图 2　热风速计系统控制电路

Fig.2　Conditioning control circuit of the sensor system

Thereafter, the heat is transmit to the ceramic substrate. One part of the heat is the horizontal heat conduction through the ceramic and aluminum ring to the outside environment. The other part of the heat is the longitudinal heat transfer to the outside environment by the heat convection.

2　Construction of the system-level model

2.1　Thermal-electric model of the sensor structure

Fig.3 shows the top view of the wind sensor. The blue part is the sensor chip, the white part is the ceramic substrate, and the grey part is the aluminum ring. L_s is the length of the chip, r_c is the radius of the ceramic substrate, and r_{Al} is the outside radius of the aluminum ring. Due to the high thermal conductivity of silicon (150 W/(m · K)) and the small size (4 mm), the temperature of the chip is simplified equal everywhere, as T_{chp}. Because the thicknesses of the chip and ceramic substrate are far less than the length of them, the same zones in the vertical direction of the chip and the ceramic substrate have approximately the same temperature. For simplicity, the shape of the chip transforms from

a square to a circle, whose radius is r_s. T_{crm} is the temperature of the outside radius of the ceramic substrate, and T_{amb} is the ambient temperature. The heat flow transfers from the center point to the outside, as shown by the yellow arrows in Fig.3.

With the thought of the lumped parameters, an analogy is drawn between the heat flow and the electric current. The voltage is an analogy for the temperature. The thermal resistance is the resistance in the thermal transfer like the resistance in the circuit. By the definition of the thermal resistance of the single layer cylindrical wall[23], the thermal resistance of the ceramic substrate is

$$R_1=\frac{\ln(r_c/r_s)}{2\pi k_c d_c} \tag{1}$$

The thermal resistance of the aluminum ring is

$$R_2=\frac{\ln(r_{Al}/r_c)}{2\pi k_{Al} d_{Al}} \tag{2}$$

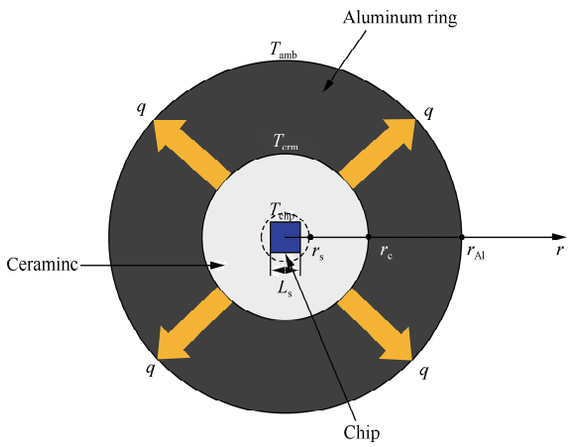

图 3 传感器顶视图

Fig.3 Top view of the sensor

where k_c is the thermal conductivity of the ceramic substrate, k_{Al} is the thermal conductivity of the aluminum ring, d_c is the the thickness of the ceramic substrate, and d_{Al} is the thickness of the aluminum ring.

According to the heat transfer coefficient formula of the flat heating surface[16], the convection coefficient of the wind sensor is

$$h_f=0.664Mk_f^{\frac{2}{3}}\mu^{-\frac{1}{6}}\rho^{\frac{1}{2}}c_p^{\frac{1}{3}}U^{\frac{1}{2}} \tag{3}$$

where M is a constant which is related to the geometric information of the sensor system. c_p, ρ, k_f, and μ are the specific heat capacity, density, heat conductivity and dynamic viscosity of the airflow, respectively. U is the velocity of the flow. The thermal resistance of the thermal convection is

$$R_f=\frac{1}{h_f A}=\frac{1}{h_f\pi r_c^2}=\frac{k_f^{-\frac{2}{3}}\mu^{\frac{1}{6}}\rho^{-\frac{1}{2}}c_p^{-\frac{1}{3}}}{0.664\pi M r_c^2}U^{-\frac{1}{2}} \tag{4}$$

Base on the thought of the lumped parameters, Fig.4 shows the thermal-electric equivalent circuit. The voltage source represents the temperature difference ΔT between the chip temperature T_{chp} and the ambient temperature T_{amb}. The T_{amb} is equal to GND. The heat flow q transfers from T_{chp} to GND through two branches in parallel. One is the branch with R_1 and R_2 in series representing the thermal conduction, the other is the R_f branch representing the thermal convection. According to Kirchhoff's current theorem, the relationship of ΔT and thermal resistances are written as

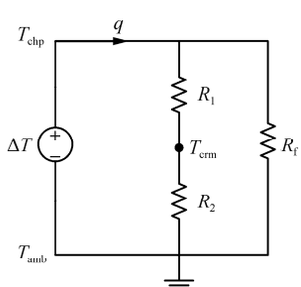

T_{chp}—the temperature of the chip; T_{amb}—the ambient temperature; T_{crm}—the temperature of the outside of the ceramic substrate; q—the thermal flow.

图 4 热学-电学等效电路

Fig.4 Thermal-electric equivalent circuit

$$q=\frac{\Delta T}{R_1+R_2}+\frac{\Delta T}{R_f} \tag{5}$$

Substitute Eq. (1), Eq. (2) and Eq. (4) into Eq. (5), the formula can be rewritten as

$$\frac{q}{\Delta T}=\frac{2\pi k_c d_c k_{Al} d_{Al}}{k_{Al} d_{Al} \ln (r_c/r_s) + k_c d_c \ln(r_{Al}/r_c)}+0.664\pi M r_c^2 k_f^{\frac{2}{3}} \mu^{-\frac{1}{6}} \rho^{\frac{1}{2}} c_p^{\frac{1}{3}} U^{\frac{1}{2}} \tag{6}$$

Evidently, $q/\Delta T$, the total thermal-electrical conductance of the sensor system, is the linear function of $U^{1/2}$.

If the material parameters and structure size are considered constant, Eq. (6) can be simplified as

$$\frac{q}{\Delta T}=A+BU^{\frac{1}{2}} \tag{7}$$

Here, $A=\frac{2\pi k_c d_c k_{Al} d_{Al}}{k_{Al} d_{Al} \ln (r_c/r_s) + k_c d_c \ln(r_{Al}/r_c)}$, $B=0.664\pi M r_c^2 k_f^{\frac{2}{3}} \mu^{-\frac{1}{6}} \rho^{\frac{1}{2}} c_p^{\frac{1}{3}}$.

To extract the parameters of the thermal-electrical model of the sensor, i. e. A and B, the experiment is performed in a wind tunnel. The sensor is heated by a voltage source with voltage ranging from 3 V to 8 V. The ambient temperature is 298 K. The wind velocity varies from 1 m/s to 20 m/s. The four heaters on the chip connect to the voltage source in parallel. The resistance of each heater is 400 Ω. The temperature of the chip is measured by the center diode on the chip. The temperature of the ambient flow is measured by the outside diode. Fig.5 shows the measurement results of the temperature difference ΔT. Fig.5(a) shows that the temperature difference ΔT with different powers decreases with the wind speed U. Fig. 5(b) shows that the temperature difference ΔT with different wind speeds increases linearly with the heat power P.

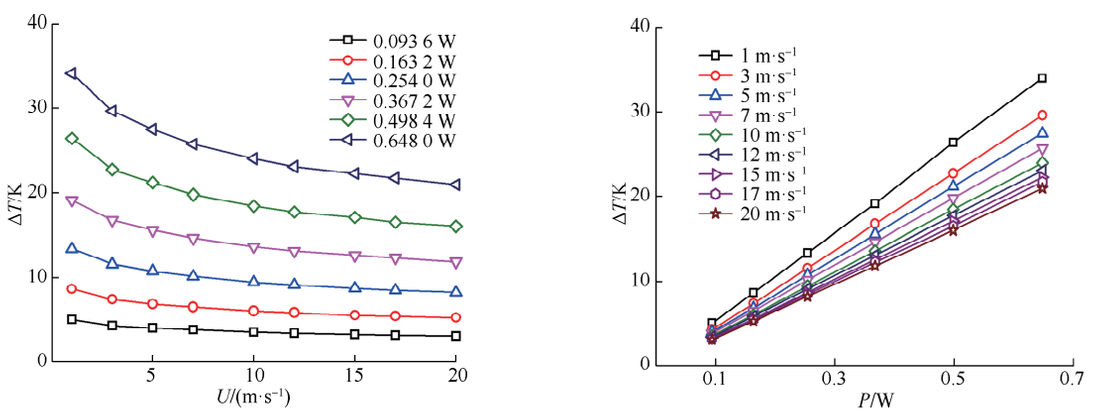

(a) Relation curve between temperature difference and wind speed

(b) Relation curve between temperature difference and heating power

图 5　温度差的测量结果

Fig.5　Measurement results of the temperature difference

According to the test data in Fig.5, with $U^{1/2}$ as the horizontal axis and $P/\Delta T$ as the vertical axis, the relationship curves under different heating powers are drawn in Fig.6. It is obvious that the different curves with different heat powers approximately coincide, and the $P/\Delta T$ is a linear function of $U^{1/2}$. The linear fitting equation can be expressed as

$$\frac{P}{\Delta T}=0.015\ 79+0.003\ 43U^{\frac{1}{2}} \tag{8}$$

In the thermal-electric model, P is the thermal flow which is equal to q in Eq. (7), ΔT is the temperature difference, and $P/\Delta T$ is the thermal conductance. Fig.4 has shown that the thermal conductance consists of two parts, one is the thermal conductance of thermal conduction, the other is the

thermal conductance of thermal convection. The thermal conductance of thermal conduction is the intercept of this linear fitting equation, 0.015 79 W/K. Then the thermal resistance of the thermal conduction R_c ($R_c=R_1+R_2$) is 63.33 K/W. The thermal conductance of thermal convection is $0.003\ 43U^{1/2}$ W/K. The thermal resistance of the thermal convection R_f is $291.5U^{-1/2}$ K/W.

In the wind sensor system, four heaters connected in parallel are powered by the heat voltage V_h, and then the heat generated transfers to the whole sensor chip, as shown in Fig. 7. In the thermal-electric model of the sensor structure, a voltage controlled current source is used to build a bridge between the electric domain and the heat domain. The controlled characteristic is the amplitude of the current source $P=V_h^2/R_h$. Here R_h is the resistance of the four heaters in parallel. The heat voltage V_h is controlled by the conditioning control circuit.

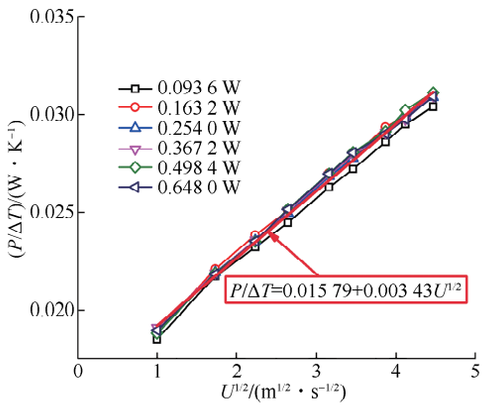

图 6 $P/\Delta T$ 与 $U^{1/2}$ 之间的关系图

Fig.6 Relationship between $P/\Delta T$ and $U^{1/2}$

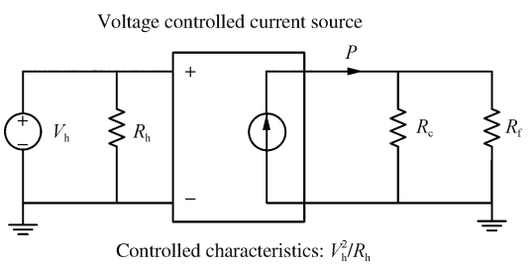

图 7 传感器结构的热学-电学模型

Fig.7 Thermal-electric model of the sensor structure

2.2 The thermal-electric model of the diodes

The temperature of the sensor is measured by the diode in the center of the chip. While the ambient temperature is measured by the outside diode. The voltage drop of the diode is a function of the temperature, as shown in Fig.8. Each diode connects with the current source, and the current is 1 mA. The test is performed in a temperature controller.

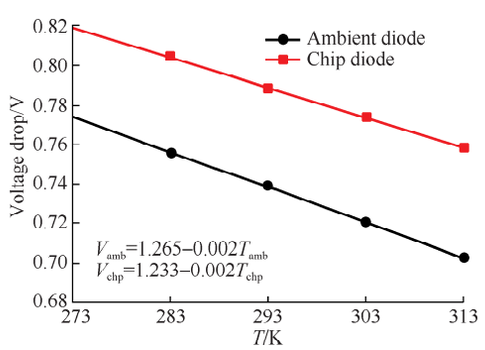

图 8 环境传感器和芯片二极管测量的电压降

Fig.8 Measured voltage drop of the ambient diode and the chip diode

Fig. 8 plots the voltage drop of the diode linearly decreasing with temperature. The linear fitting function of the diode on the chip can be expressed as

$$V_{chp}=1.233-0.002T_{chp} \tag{9}$$

The linear fitting function of the outside diode can be written as

$$V_{amb}=1.265-0.002T_{amb} \tag{10}$$

where T_{chp} and T_{amb} are in K. The difference between these two linear fitting functions is the cause of encapsulation.

In the same way, the voltage is an analogy for the temperature. The thermal-electric model of the

diode is a voltage controlled voltage source shown in Fig. 9. The DC power is the real temperature in K. GND represents 273 K. The voltage controlled voltage source converts the temperature into the voltage.

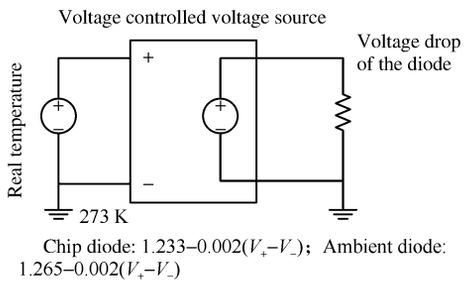

图 9　二极管的热学-电学模型

Fig. 9　Thermal-electric model of the diode

2.3　The system-level model

The thermal-electric model of the sensor structure, the thermal-electric model of the ambient diode and chip diode, and the conditioning circuit are connected to form the system-level model, shown in Fig. 10. The left part is the thermal-electric model of the flow sensor. Then the right part is the electronic interface. In the original conditioning circuit shown in Fig. 2, the chip diode and the environment diode in the Wheatstone bridge are replaced by the thermal-electric model of these two diodes. The voltage drop of the ambient diode V_{amb} is controlled by the ambient temperature T_{amb}. And the voltage drop of the chip diode V_{chp} is controlled by the chip temperature T_{chp}. The temperature difference $\Delta T = T_{chp} - T_{amb}$. In the original conditioning circuit, the heating resistor is replaced by the thermal-electric model of the sensor structure. And in the thermal-electric model of the sensor structure, the voltage of the output end of the controlled current source is ΔT.

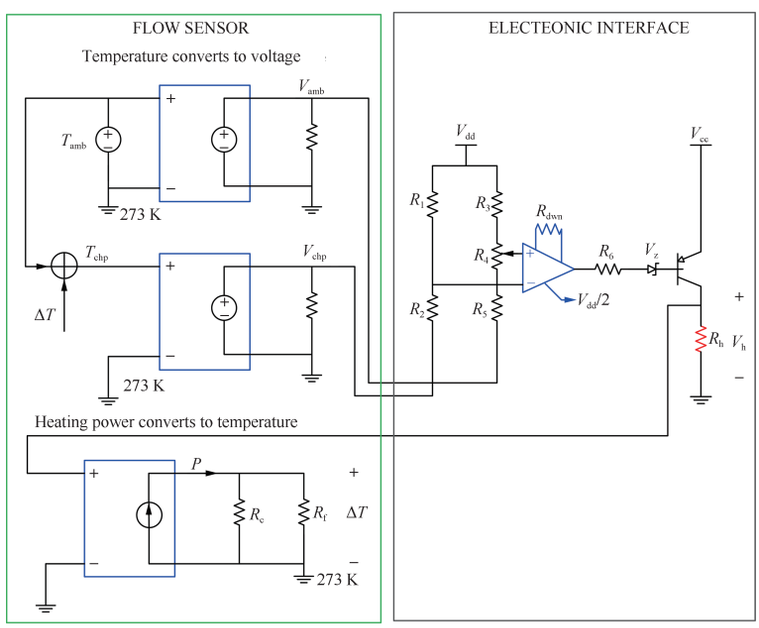

图 10　传感器系统的系统级模型

Fig. 10　System-level model of the sensor system.

To keep the temperature difference between the chip temperature and the ambient temperature 293 K, the circuit parameters are set as $R_1 = 2.7$ kΩ, $R_2 = 2$ kΩ, $R_3 = 1.5$ kΩ, $R_4 = 2$ kΩ, $R_5 = 1$ kΩ, $R_6 = 5.1$ kΩ, $R_{dwn} = 200$ Ω, $R_h = 100$ Ω, $V_z = 7.5$ V, $V_{dd} = 5$ V, $V_{cc} = 12$ V, $R_c = 63.33$ K/W, $R_f = 291.5U^{-1/2}$ K/W.

3　Experiments

Circuit simulation experiments are executed in Cadence. To simulate the wind speed varies from

1 m/s to 40 m/s, R_f is set as 291.5, 168.3, 130.4, 110.2, 87.9, 75.3, 65.2, 58.3, 53.2, 49.3, 46.1 Ω, corresponding to the wind speed 1, 3, 5, 7, 11, 15, 20, 25, 30, 35, 40 m/s, respectively. T_{amb}=287 K. By changing R_f, the heating voltage V_h corresponding to different wind speeds is tested. The simulation results are drawn by the black curve in Fig.11. With the increase of the wind speed, the heating voltage increases, which is consistent with the theoretical analysis of the conditioning control circuit in Sec. 1.

The measurement experiments are performed in the wind tunnel. The ambient temperature is set as 287 K, and the wind speed varies from 1 m/s to 40 m/s. The measurement results are drawn by the red curve in Fig.11. The measurement results are nearly consistent with the simulation results. The percentage errors between the simulation results and the measurement results in different wind speed are given in Table 1. Table 1 indicates that the percentage error is less than 1.56%, the system-level model of the sensor system viable and feasible.

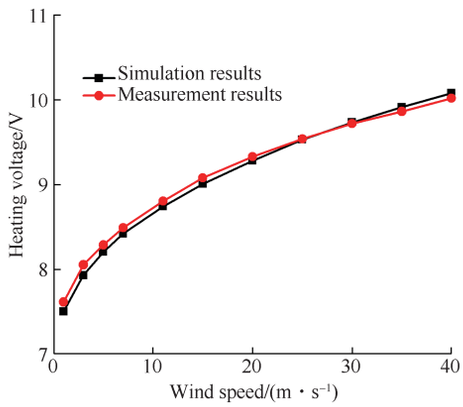

图 11 加热电压随风速变化图

Fig. 11 Diagram of heating voltage variation with wind speed

表 1 仿真结果与测量结果之间的误差

Table 1 Percentage errors between the simulation results and the measurement results

Wind speed/ (m · s^{-1})	1	3	5	7	11	15	20	25	30	35	40
Error/%	1.53	1.56	1.00	0.83	0.75	0.78	0.52	0.08	−0.15	−0.51	−0.58

4 Conclusion

This paper has presented a system-level model of the wind sensor system. The system-level model is based on theory of lumped parameters. The thermal-electric model of the sensor structure was constructed by a voltage controlled current source in which the controlled current source presented the heat flow produced by heating four heaters. The function of thermal conduction and thermal convection were expressed by two resistors. The thermal-electric model of the diode was constructed by a voltage controlled voltage source in which the controlled voltage source presented the voltage across the diode. Combining the thermal-electric models with the conditioning control circuit, the system-level model of the wind sensor system was constructed. The simulation results of the system-level showed a good agreement with the measurement results. The percentage error was less than 1.56%. The results presented here provide a valuable reference for the practical application of the wind sensor.

References:

[1] ZHU Y Q, CHEN B, QIN M, et al. 2-D micromachined thermal wind sensors-a review[J]. IEEE Internet of Things Journal, 2014, 1(3): 216-232.

[2] BRUSCHI P, DILIGENTI A, NAVARRINI D, et al. A double heater integrated gas flow sensor with thermal feedback[J]. Sensors and Actuators A: Physical, 2005, 123/124: 210-215.

[3] LIU C，HUANG J B. A micromachined flow shear-stress sensor based on thermal transfer principles[J]. Journal of Microelectromechanical Systems：A Joint IEEE and ASME Publication on Microstructures，Microactuators，Microsensors，and Microsystems，1999，8(1)：90-99.

[4] YE Y Z，YI Z X，GAO S X，et al. Effect of insulation trenches on micromachined silicon thermal wind sensors[J]. IEEE Sensors Journal，2017，17(24)：8324-8331.

[5] YE Y Z，YI Z X，GAO S X，et al. DRIE trenches and full-bridges for improving sensitivity of 2-D micromachined silicon thermal wind sensor[J]. Journal of Microelectromechanical Systems，2017，26(5)：1073-1081.

[6] CUBUKCU A S，ZERNICKEL E，BUERKLIN U，et al. A 2D thermal flow sensor with sub-mW power consumption[J]. Sensors and Actuators A：Physical，2010，163(2)：449-456.

[7] ZHU Y Q，CHEN B，GAO D，et al. A robust and low-power 2-D thermal wind sensor based on a glass-in-silicon reflow process[J]. Microsystem Technologies，2016，22(1)：151-162.

[8] HOURDAKIS E，SARAFIS P，NASSIOPOULOU A G. Novel air flow meter for an automobile engine using a Si sensor with porous Si thermal isolation[J]. Sensors (Basel，Switzerland)，2012，12(11)：14838-14850.

[9] BREVET W，SEBASTIANO F，MAKINWA K. A 25 mW smart CMOS wind sensor with corner heaters[C]//IECON 2015-41st Annual Conference of the IEEE Industrial Electronics Society. Yokohama：IEEE，2015：1194-1199.

[10] SABATÉ N，SANTANDER J，FONSECA L，et al. Multi-range silicon micromachined flow sensor[J]. Sensors and Actuators A：Physical，2004，110(1/2/3)：282-288.

[11] ZHU Y Q，QIN M，YE Y Z，et al. Modelling and characterization of a robust，low-power and wide-range thermal wind sensor[J]. Microsystem Technologies，2017，23(12)：5571-5585.

[12] CERIMOVIC S，TALIC A，BEIGELBECK R，et al. Bidirectional micromachined flow sensor featuring a hot film made of amorphous germanium[J]. Measurement Science and Technology，2013，24(8)：084002.

[13] ASHAUER M，GLOSCH H，HEDRICH F，et al. Thermal flow sensor for liquids and gases based on combinations of two principles[J]. Sensors and Actuators A：Physical，1999，73(1/2)：7-13.

[14] WANG S，YI Z X，QIN M，et al. Temperature effects of a ceramic MEMS thermal wind sensor based on a temperature-balanced mode[J]. IEEE Sensors Journal，2019，19(17)：7254-7260.

[15] GAO S X，YI Z X，YE Y Z，et al. Temperature effect and its compensation of a micromachined 2-D anemometer [J]. IEEE Sensors Journal，2019，19(14)：5454-5459.

[16] HUANG Q G，CHEN B，ZHU Y Q，et al. Modeling of temperature effects on micromachined silicon thermal wind sensors[J]. Journal of Microelectromechanical Systems，2015，24(6)：2033-2039.

[17] CHEN B，ZHU Y Q，YI Z X，et al. Temperature effects on the wind direction measurement of 2D solid thermal wind sensors[J]. Sensors (Basel，Switzerland)，2015，15(12)：29871-29881.

[18] YI Z X，WANG D，QIN M，et al. Encapsulation glue effect of encapsulation glue on micromachined thermal wind sensor[J]. IEEE Sensors Letters，2018，2(4)：1-3.

[19] KOWALSKI L，RICART J，JIMÉNEZ V，et al. Thermal modelling of the chip for the REMS wind sensor[J]. International Journal of Numerical Modelling：Electronic Networks，Devices and Fields，2010，23(4)：340-353.

[20] DALOLA S，CERIMOVIC S，KOHL F，et al. MEMS thermal flow sensor with smart electronic interface circuit [J]. IEEE Sensors Journal，2012，12(12)：3318-3328.

[21] SOSNA C，BUCHNER R，LANG W. A temperature compensation circuit for thermal flow sensors operated in constant-temperature-difference mode[J]. IEEE Transactions on Instrumentation and Measurement，2010，59(6)：1715-1721.

[22] SHEN G P，QIN M，HUANG Q G. A system-level model for a silicon thermal flow sensor[J]. Microsystem Technologies，2009，15(2)：279-285.

[23] ISHIZUKA M，FUKUOKA Y. Application of the thermal network method to the transient thermal analysis of multichip modules[C]//2nd 1998 IEMT/IMC Symposium (IEEE Cat. No. 98EX225). Tokyo：IEEE，1998：161-166.

（责任编辑：李艳，周安迪）